Article

Zwitterionic Surfactant Stabilized Palladium Nanoparticles as Catalysts in Aromatic Nitro Compound Reductions

Franciane D. Souza,* Haidi Fiedler and Faruk Nome*

*Departamento de Química, Universidade Federal de Santa Catarina,
88040-900 Florianópolis-SC, Brazil*

Palladium nanoparticles (NPs) stabilized by ImS3-14, a zwitterionic surfactant structurally related to ionic liquids, are revealed here to be good catalysts for the reduction of a large number of substituted aromatic nitro compounds. Our mass spectrometry results are consistent with the formation of amino products in a direct route, where the aromatic nitro compounds are initially reduced to nitroso compounds, which are then reduced to the hydroxylamine derivatives and finally to the anilines. Activation parameters showed that for most Pd catalysts reported in the literature, the mechanism seems to be similar, with lower enthalpy of activation ($\Delta H^{\ddagger}$) being compensated by more negative entropy of activation ($\Delta S^{\ddagger}$). As a result, the reaction is thermally compensated and the rate constants for most reactions rather similar. Furthermore, Pd NPs stabilized by ImS3-14 showed efficient catalytic activities for the reduction of aromatic nitro compounds, with high conversion and good selectivity even using very low loadings of metal.

Keywords: aromatic nitro reduction, mettalic nanoparticles, catalysis

Introduction

Metallic nanoparticles (NPs) play a central role in modern nanoscience because of their unique chemical and physical properties, and several methods have been developed for their synthesis.[1-6] The most common methods for their preparation involve the chemical reduction of metal salts[4,7,8] and, due to the low stability in solution of metallic nanoparticles, the synthesis is normally performed in the presence of stabilizing agents.[3,4,7-10] Surfactants are a versatile class of stabilizers, which show a broad range of polar head groups and carbon chains and can control size, shape and solubility of the nanoparticles.[11,12] Studies involving cationic, anionic and neutral surfactants in nanoparticle synthesis are well known, but the use of zwitterionic surfactants is relatively new. Early work involving zwitterionic surfactants and metallic nanoparticles by Reetz and Helbig[13] describes the synthesis of palladium nanoparticles (Pd NPs) using SB3-14 as a stabilizer. Recently we described the preparation of Pd NPs with narrow size distribution and high stability in aqueous media using 3-(1-dodecyl-3-imidazolio)propane-sulfonate (ImS3-12), a zwitterionic surfactant containing an imidazolium ring.[11,14] Similar synthesis of palladium and gold nanoparticles showing narrow size distribution used zwitterionic surfactants of the type 3-(1-alkyl-3-imidazolio) propane-sulfonate (ImS3-n, with n = 10, 12, 14 and 16, Figure 1) in organic media.[15,16]
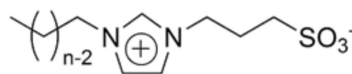

Figure 1. Chemical structure of ImS3-n surfactants.

The large proportion of their atoms on the surface makes metallic nanoparticles targets of special interest for application in catalysis.[3,8,17] The size,[9,18-21] shape,[12,22] surface properties[9] and environments[5,9,23] of metal nanoparticles can all have a significant effect on their catalytic activity. The stabilizer plays an important role because it can reduce the catalytic activity of the nanoparticle by hindering substrate contact or by blocking product departure from the surface.[24-26] Thus, there is a growing need for the development of new methods for the synthesis of well-dispersed nanoparticles and for stabilizers which do not affect the catalytic activity.

The reduction of aromatic nitro compounds to anilines is an important process because they are useful precursors and intermediates in the preparation of dyes, polymers, pharmaceutical substances, agricultural chemicals and

---

*e-mail: franciane_dutra@hotmail.com, faruk.nome@ufsc.br

other products. Additionally, anilines appear in numerous natural products and display a wide range of biological activities.[2,10,27-30] Moreover, nitro compounds are often highly toxic and not readily biodegradable.[10,30,31] Reduction to anilines produces compounds which are much less toxic and easily biodegradable. There is no shortage of methods to realize this reduction process,[2,27,29,32-36] but the poor selective reduction of the nitro to the amino-group in the presence of other reducible functionalities can make this reaction a challenging task. Additionally, the reduction of a nitro group proceeds in a series of steps and hydroxylamine, hydrazine and azoarene side products can be obtained.[2,27,33] Due to these disadvantages, the development of new methods or the improvement of already established methods remains the focus of extensive research efforts.

In the present study, we examine the efficiency of Pd NPs prepared by chemical reduction in the presence of a zwitterionic surfactant of the ImS3-n family, which is structurally related to ionic liquids. The catalytic activity of the Pd NPs was initially tested in the reduction of 4-nitrophenol by $NaBH_4$, a reaction which can be conveniently followed by UV-Vis spectroscopy.[6,37,38] After optimization, the reduction reaction was examined for a large number of aromatic nitro compounds with different substituents. Finally, a catalytic mechanism for the reduction reaction is proposed, based on the evidence obtained applying electrospray ionization tandem mass spectrometry [ESI-MS(/MS)] in negative ion mode to monitor the course of reaction, which allowed us to detect several intermediates.

Results and Discussion

Preparation and quantification of palladium nanoparticles

Reverse micelles can be used as nanoreactors for the synthesis of metallic nanoparticles due to the constrained environment provided by this system. In fact, ImS3-14 was used to prepare palladium nanoparticles by mixing a reverse micelle solution containing 0.05 mol L^{-1} ImS3-14 and an aliquot of 0.2 mol L^{-1} K_2PdCl_4 aqueous solution in chloroform with a solution containing 0.05 mol L^{-1} ImS3-14 and an aliquot of 2.0 mol L^{-1} ascorbic acid as the reductant. The water to surfactant concentration ratios, w_0, used for the preparation of Pd NPs were $w_0 = 4.8$ (Pd NPs 1)[15] and $w_0 = 14.7$ (Pd NPs 2).[39,40] The Pd NPs obtained were characterized by transmission electronic microscopy (TEM) and images showed that the NPs are well dispersed and show no sign of aggregation (see Figure S1 in the Supplementary Information (SI) section). The mean diameters of the nanoparticles obtained on the

basis of TEM image analysis of ca. 300 particles are shown in Table 1. The increase in w_0 results in an increase of the nanoparticle diameter, proving the influence of reverse micelle media in nanoparticle synthesis.[15]

Table 1. Size and concentration of palladium in Pd NPs solutions

	Diameter / nm	[Palladium][a] / ppm
Pd NPs 1	4.2 ± 1.0[b]	40.7
Pd NPs 2	5.8 ± 2.0[c]	125.0

[a]Measured by energy dispersive X-ray fluorescence; [b]value taken from reference 16; [c]value taken from reference 15.

The concentration of palladium in the Pd NPs in solution was determined by energy dispersive X-ray fluorescence (EDXRF), a non-destructive technique which is ideal for analyzing liquid or solid samples with limits of detection in the ppm scale: the results are given in Table 1.[40] Since all the catalytic tests were performed in aqueous media, chloroform removal and nanoparticle dispersion in aqueous media was necessary before using the Pd NPs prepared in reverse micelles. Dispersion of Pd NPs in pure water was not possible and a 0.08 mol L^{-1} NaCl aqueous solution was used to solubilize the nanoparticles in aqueous media. The Pd NPs showed long-term stability, without signs of precipitation or aggregation (Figure 2).
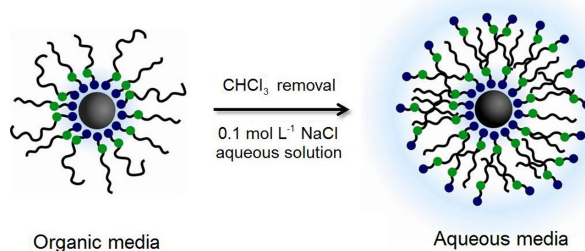
Figure 2. Cartoon model of the change in stabilization mechanism of Pd NPs by ImS3-14 surfactant in organic and in aqueous media.

Reduction of 4-nitrophenol catalyzed by palladium nanoparticles

The catalytic activity of the different Pd NPs was compared using the reduction of 4-nitrophenol (Nip) to 4-aminophenol (Amp), in the presence of $NaBH_4$ (the [$NaBH_4$] exceeds the Nip and catalyst concentrations).[6] The reaction can be conveniently monitored in the UV-Vis region, following the disappearance of 4-nitrophenolate ion at 400 nm, and the formation of a new absorption band around 300 nm, attributed to the formation of Amp.[6] Figure 3a shows typical spectral changes observed as a function of time in the presence of Pd NPs 1 and Figure 3b
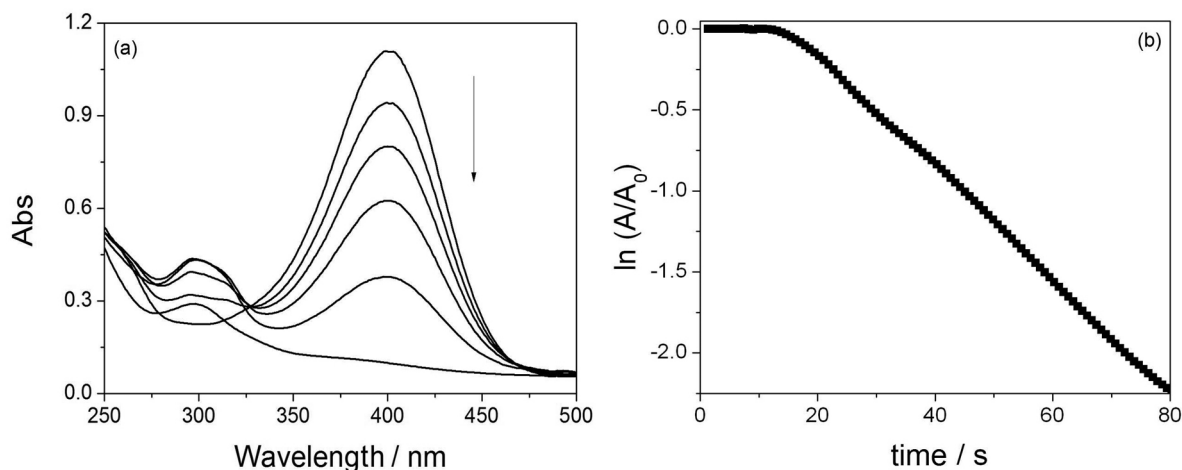
Figure 3. (a) Variation in UV-Vis absorption spectra of reduction of 4-nitrophenol (0.066 mmol L^{-1}) with NaBH$_4$ (9.71 mmol L^{-1}) catalyzed by palladium nanoparticles (Pd NPs 1-0.0167 mmol L^{-1}) ([NaCl] = 0.033 mmol L^{-1}). (b) Time-dependence of the absorption of 4-nitrophenolate ions at 400 nm ([4-nitrophenol] = 0.066 mmol L^{-1}; [NaBH$_4$] = 9.71 mmol L^{-1}; [Pd NPs 1] = 0.0167 mmol L^{-1}, [NaCl] = 0.033 mmol L^{-1}). All reactions were carried at 25 °C.

shows the time dependence of the reduction of Nip at 400 nm.[6,37,38] In the absence of the Pd NPs 1 catalyst, the absorbance at 400 nm remains unaltered. Similar spectral changes were obtained for all the Pd NPs systems studied.

In these reactions, after the addition of NaBH$_4$ there is a short induction time,[6,37] common to heterogeneous catalysts and corresponding to the time required for catalyst activation. This induction time has been attributed to such factors as the diffusion-controlled adsorption of substrates on the nanoparticle surface; the presence of dissolved oxygen in water reacting faster with BH$_4^-$ than the reaction of borohydride with Nip, poisoning of the nanoparticle surface by a metal oxide layer and the slow surface restructuring of the nanoparticles.[6,37,38,41,42]

The absence of a well-defined isosbestic point in Figure 3a indicates that Nip is not converted to Amp in a single step and, as can be seen in Figure S2 (SI section), the changes in the UV spectra are complex. In fact, following the absorbance changes in 296 nm, which is the wavelength corresponding to the formation of Amp, an initial increase in absorbance reaches a maximum

before falling (Figure S3 in SI section), with the maximum indicative of the presence of 4-hydroxylaminophenol, which is expected to show absorbance near 300 nm, before being further reduced to Amp. The observed profile indicates that reduction occurs in several steps, where the intermediates leave the nanoparticle surface after reduction then return to the surface for subsequent steps of the reduction to 4-aminophenol. According to Figure 4, the reaction proceeds in three steps: the very fast reduction of Nip to 4-nitrosophenol and then to 4-hydroxylaminophenol, which is reduced to the aniline in the final, slowest step. In order to confirm the UV-visible analysis, we performed some mass spectrometry experiments.

Mass spectrometric study of the Nip reduction

The reduction of Nip by BH$_4^-$ catalyzed by palladium nanoparticles was confirmed performing ESI-MS experiments, with the equipment operating in negative ion mode. Figure 5 shows the ESI(−)-MS spectrum of an aliquot taken after the addition of NaBH$_4$ solution to the
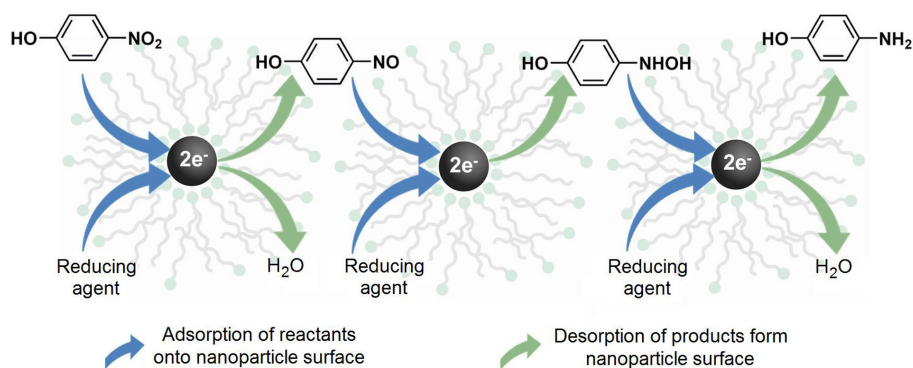
Figure 4. Cartoon model describing the reduction of 4-nitrophenol and intermediates on the nanoparticle surface.

solution containing Nip and palladium nanoparticles. The reduction was carried out with lower Pd NP concentration to slow the reactions and allow the detection of the reaction intermediates. Several peaks were observed, consistent with the products and intermediates of the reaction according to Figure 4. However, no signal corresponding to 4-nitrosophenolate was detected, indicating that this particular intermediate is consumed very fast.
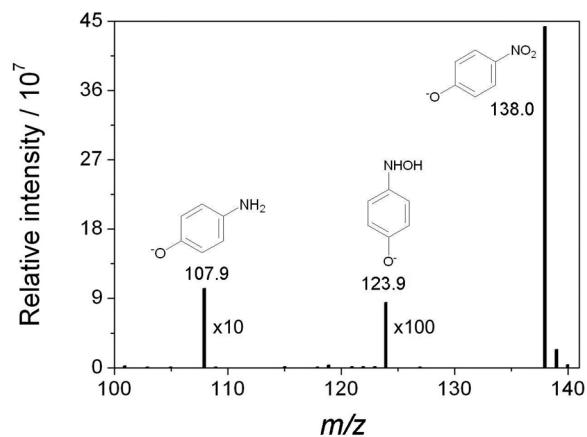
Figure 5. ESI-MS spectrum in negative ion mode of an aliquot taken after 5 min of reaction in the presence of Pd NPs. The reaction conditions were [Nip] = 0.093 mmol L^{-1}; [NaBH$_4$] = 9.71 mmol L^{-1}; [NaCl] = 0.033 mmol L^{-1}; [Pd] = 0.0019 mmol L^{-1} and aliquots were diluted ten times and injected in the mass spectrometer.

The presence of the intermediates is strong evidence that after each step of the reduction, the organic intermediates leave the surface of the nanoparticle, allowing both recovery of the surface and detection of the intermediates by ESI-MS. In fact, mass spectrometric analysis using ESI-MS in the negative mode monitors the reaction collecting snapshots of its anionic composition. Reagent, intermediates and products present as anions are expected to be transferred directly from the reaction solution to the gas phase and then detected by ESI-MS. The peak at *m/z* 138.0 refers to the deprotonated 4-nitrophenoxide ion and the *m/z* 107.9 fragment indicates the formation of 4-aminophenolate, the final product of reaction. Furthermore, in this spectrum, we detected the deprotonated 4-hydroxyaminophenol ion of *m/z* 123.9, an intermediate of the reaction and this peak displaying a lower intensity when compared to the 4-nitrophenolate signal. The ESI(−)-MS spectrum for Pd NPs 2 and ESI(+)-MS and ESI-MS/MS spectra for both systems are shown in Figures S4 to S8 in the SI section. ESI(+)-MS and the cleavage observed in the ESI-MS/MS spectra (see SI section) showed several ions consistent with the presence of Nip (peak of *m/z* = 138.0), Amp (peak of *m/z* = 107.9) and 4-hydroxyaminophenol (peak of *m/z* = 123.9). Clearly, our results are consistent with the formation of amino products in a direct route, where the

aromatic nitro compounds are initially reduced to nitroso compounds, which are then reduced to the hydroxylamine derivatives and finally to the anilines.

Kinetic study of the Nip reduction

As the concentration of borohydride remains essentially constant during the reaction, the pseudo first order analysis could be used to evaluate the catalytic rate. The apparent pseudo first order rate constants (k$_{app}$) were determined from the slope of the linear correlation of ln(A/A$_0$) with time t, shown in Figure 3b and the values of k$_{app}$ as a function of the concentrations of 4-nitrophenol and sodium borohydride are shown in Figure 6. As shown in Figure 6a, an increase in the concentration of Nip leads to a decrease in the value of the experimental pseudo first order rate constant (k$_{app}$) and the effect is observed with both Pd NPs, being slightly more pronounced in the presence of the smaller Pd NPs 1. As expected, the effect is related to the bigger surface area of these nanoparticles, when compared with the same concentration of Pd NPs 2. It is interesting to note that the decrease in k$_{app}$ corresponds to the plateau region in a typical plot of initial rate *versus* [Nip] in terms of the Langmuir-Hinshelwood model, indicating that diffusion and binding of the substrates to the surface of the catalyst followed by reaction on the catalyst surface are rate limiting (see inset in Figure 6a). Conversely, as can be seen in Figure 6b, the increase in the concentration of NaBH$_4$ leads to an increase in k$_{app}$ and the diameter of nanoparticle has no effect on the rate profile, indicating that recovery of the catalytic surface, via reduction with NaBH$_4$ play a fundamental role.[6,37]

The explanation for the characteristic dependence of k$_{app}$ on the concentration of Nip and BH$_4^-$ is that both reactants compete for free places on the nanoparticle surface and the reaction takes place only between adsorbed species on the surface. If most places are occupied by a single species, the reaction rate will be decreased. This is observed at higher concentrations of Nip.[6,37,38]

The k$_{app}$ is found to be proportional to the total surface area available in the metal nanoparticle and associated with zero-order reaction dependence with respect to BH$_4^-$.[41] Thus, the rate of reduction of Nip can be defined by equation 1:[6,37,41]

$$\frac{dc_{Nip}}{dt} = k_{app}c_{Nip} = k_1 S c_{Nip} \tag{1}$$

where k$_{app}$ is the apparent rate constant, k$_1$ is the rate constant normalized to S, the total surface area of metal nanoparticles normalized to the unit volume of the reaction system. Figure 7 shows the plots of k$_{app}$ as a function of the surface area S for palladium nanoparticles. The rate
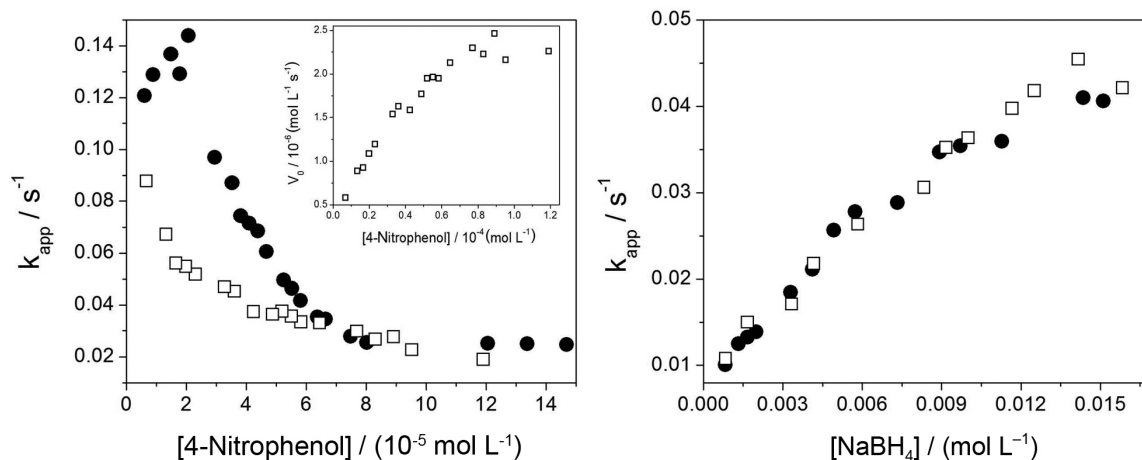
Figure 6. (a) Dependence of the apparent rate constant k_{app} on the concentration of Nip at $[BH_4^-] = 9.71$ mmol L^{-1}; $[NaCl] = 0.033$ mmol L^{-1}; $[Pd] = 0.0167$ mmol L^{-1}. The insert shows the dependence of initial rate on the concentration of Nip; (b) dependence of the apparent rate constant k_{app} on the concentration of BH_4^- at $[Nip] = 0.093$ mmol L^{-1}; $[NaCl] = 0.033$ mmol L^{-1}; $[Pd] = 0.0167$ mmol L^{-1}. ($\bullet$) Pd NPs 1 ($S = 0.21$ m^2 L^{-1}); ($\square$) Pd NPs 2 ($S = 0.14$ m^2 L^{-1}). All reactions were carried at 25 °C.

constant k_1 obtained for Pd NPs 1 = 0.142 s^{-1} m^{-2} L and for Pd NPs 2 = 0.299 s^{-1} m^{-2} L. The Pd NPs 2 showed a higher catalytic activity than Pd NPs 1, indicating the influence of nanoparticle size on the catalytic activity.

Thermodynamic parameters

Thermodynamic parameters measured for the reduction reactions of Nip in the presence of Pd NPs 1 and Pd NPs 2, are summarized in Table 2 and were calculated using standard equations described in the experimental section and values of the apparent rate constant (k_{app}) at different temperatures given in the SI section (Figure S9 in the SI section).

Table 2 compares activation parameters for the Nip reduction reaction in the presence of Pd NPs with several other systems. For both nanoparticles and for other systems reported in the literature (Table 2), negative values of $\Delta S^{\ddagger}$ were obtained, probably due to a more ordered structure in the transition state related to the adsorption of Nip onto the
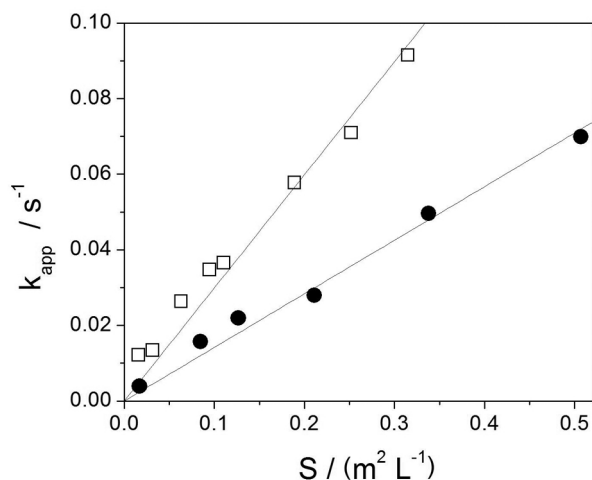
Figure 7. Apparent rate constant k_{app} as a function of the surface area normalized to the unit volume of the reaction system S for palladium nanoparticles ([4-nitrophenol] = 0.093 mmol L^{-1}; $[BH_4^-] = 9.71$ mmol L^{-1}; $[NaCl] = 0.033$ mmol L^{-1}, at 25 °C). ($\bullet$) Pd NPs 1; ($\square$) Pd NPs 2.

surface of palladium nanoparticles.[43] In general, the reaction seems to be thermally compensated and, as can be seen in

Table 2. Thermodynamic parameters for the Nip reduction catalyzed by palladium

Catalyst	$\Delta H^{\ddagger}$ / (kJ mol^{-1})	$\Delta S^{\ddagger}$ / (J mol^{-1} K^{-1})	$\Delta G^{\ddagger}$ / (kJ mol^{-1})	E_a / (kJ mol^{-1})	Reference
Pd NPs 1	45.94	−127.4	83.50	48.5	This work
Pd NPs 2	50.66	−111.8	83.97	53.2	This work
G4-OH(Pd$_{40}$)	43.8	−158.0	90.9	50.9	43
G5-OH(Pd$_{80}$)	40.6	−163.6	89.3	46.9	43
G6-OH(Pd$_{160}$)	16.4	−240.8	88.2	17.9	43
Pd$_{13}$DENs	29	−198	88	30.6	44
Pd$_{55}$DENs	27	−204	88	31.4	44

$\Delta H^{\ddagger}$: enthalpy of activation; $\Delta S^{\ddagger}$: entropy of activation; $\Delta G^{\ddagger}$: Gibbs energy of activation; E_a: energy of activation.

Figure 8, lower activation enthalpies lead to more negative entropies of activation (which is equivalent to higher values of the Arrhenius A term). As a result of the thermal compensation, although the change in enthalpy of activation is about 30 kJ mol^{-1}, the free energies of activation do not reflect directly the change (Figure 8) and there is a much smaller difference in rate constant (and free energies of activation) than expected in terms of the enthalpy changes.
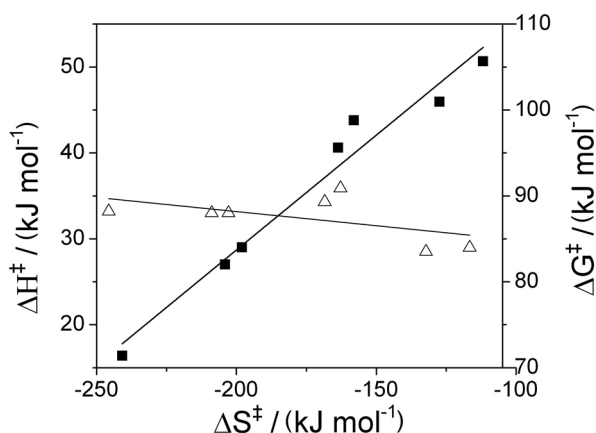
Figure 8. Enthalpy (■) and free energy (△) of activation as a function of the change in entropy of activation, showing a typical thermal compensation reaction for the reduction using different palladium systems as catalysts.

Reduction of aromatic nitro compounds

To evaluate the scope and limitations of the Pd NPs, several substituted aromatic nitro compounds were tested to verify the reduction to anilines. Initially, the reduction of mono substituted aromatic nitro compounds by NaBH$_4$ in a fixed time of 30 min were tested (Table 3) and the conversions obtained were, in all cases 100%, except for 3-nitroaniline with Pd NPs 2 which was 83%. These results indicate that the position of the substituents had little or no effect on the reactivity.

In a second set of experiments, the reduction of halo-substituted aromatic nitro compounds with one or two substituents were evaluated (Table 4). All the reactions showed 100% conversion of reagents to products. However, in some cases, other products were formed besides the expected aniline derivative. For 4-bromonitrobenzene, dehalogenation and the formation of azo products was observed. In the case of 2-bromo-4-nitrophenol, debrominated product was found in the reduction using Pd NPs 1 as catalyst. Reactions of the iodonitrobenzenes produced a complex mixture of dehalogenated and azo products and was not analyzed in detail. Although Pd catalysts are known to show a high tendency to catalyze halogen displacement;[45-48] in this work, dehalogenated

Table 3. Reduction of mono substituted aromatic nitro compounds catalyzed by palladium nanoparticles[a]

Substituent X	Pd NPs 1 Conversion / %	Pd NPs 2 Conversion / %	TON
H			
2-OH			
3-OH			
4-OH	100	100	100
2-NH$_2$			
4-NH$_2$			
4-CH$_2$OH			
3-NH$_2$	100	83	83[b]

[a]All the reactions were carried out nitro using (0.05 mmol) of the aromatic nitro compound, 1 mol% of Pd NPs, 11 equivalents of NaBH$_4$ and 9.9 mL of THF/H$_2$O (1:2.3); [b]TON (ratio of moles of desired product formed to moles of catalyst) calculated using the amount product formed in 30 min.
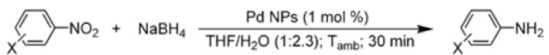
Table 4. Reduction of halo-substituted nitro aryl compounds catalyzed by palladium nanoparticles[a]

Substituents X,Y	Pd NPs 1 Selectivity[b] / %	Pd NPs 2 Selectivity[b] / %
2-F (Y=H)	100	100
4-Br (Y=H)	69	54
2-Cl-5-OH	100	100
3-Cl-4-NH$_2$	100	100
3-Br-4-OH	97	100
3-Cl-4-OH	100	100
2-I (Y=H)		
3-I (Y=H)	—[b]	—[b]
4-I (Y=H)		

[a]All the reactions were carried out using (0.05 mmol) of the aromatic nitro compound, 1 mol% of Pd NPs, 11 equivalents of NaBH$_4$ and 9.9 mL of THF/H$_2$O (1:2.3); [b]for iodo-nitrobenzene, the selectivity values are not shown because a complex mixture products was obtained.

products were obtained only with iodo derivatives and, in a minor proportion, with the bromo substituted nitro arenes.
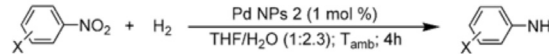
Finally, the reduction of substituted aromatic nitro compounds containing groups which can be reduced by NaBH$_4$ was evaluated (Table 5). The reduction of nitrobenzaldehydes showed that, besides the reduction of the nitro group, the aldehyde function was also reduced with formation of the corresponding aminobenzyl alcohol. In the reaction of 2-nitrobenzaldehyde, a small amount of *N*-phenylformamide was detected as side product. Finally, the reaction of 4-nitroacetophenone produced a mixture of 4-aminoacetophenone and 4-aminostyrene.

Table 5. Reduction of nitro substituted aryl compounds with other reducible group catalyzed by palladium nanoparticles[a]

Reagent substituent	Product substituent	Pd NPs 1 selectivity[b] / %	Pd NPs 2 selectivity[b] / %
4-COCH$_3$	4-COCH$_3$	43	40
2-CHO	2-CH$_2$OH	92	87
3-CHO	3-CH$_2$OH	100	100
4-CHO	4-CH$_2$OH	100	100

[a]All the reactions were carried out using (0.05 mmol) of the aromatic nitro compound, 1 mol% of Pd NPs, 11 equivalents of NaBH$_4$ and 9.9 mL of THF/H$_2$O (1:2.3).

Other milder reducing agents were tested, but hydroquinone and formic acid led to precipitation of the Pd NPs and ammonium formate was unable to reduce the nitro group after 20 h in these conditions. Using hydrogen gas, precipitation of Pd NPs 3 was observed, but Pd NPs 2 showed good conversions and selectivity for the reduction of a variety of nitroaromatic compounds (Table 6).

Table 6. Reduction of aromatic nitro compounds using Pd nanoparticles[a]

Reagent substituent	Product substituent	Conversion[d] / %	TON[b]
H	H		
4-OH	4-OH		
4-NH$_2$	4-NH$_2$		
4-CH$_2$OH	4-CH$_2$OH	100	100
4-COCH$_3$	4-COCH$_3$		
4-Br	4-H		

[a]All the reactions were carried out using (0.05 mmol) of the nitro aryl compounds, 1 mol% of Pd NPs, 4 bar of H$_2$ and 1.9 mL of THF/H$_2$O (1:2.3). TON: ratio of moles of desired product formed to moles of catalyst.

Conclusions

Pd NPs stabilized by ImS3-14 showed efficient catalytic activities for the reduction of nitroarenes in the presence of NaBH$_4$, with high conversion and good selectivity. Substituents had little or no effect on the reactivity or selectivity and azo products were observed in significant amounts only in the reactions of iodo derivatives. The reduction with H$_2$ showed good conversion and selectivity with no sign of hydroxylamine products. The reduction of 4-nitrophenol was examined by UV-visible and mass spectroscopic techniques and allowed us to understand that the reaction proceeds via nitroso and hydroxylamine derivatives, and that the intermediate molecules leave the nanoparticle surface, with the reaction proceeding in several steps where adsorption and desorption are observed in each step of the reaction. Activation parameters show that mechanisms seem to be similar for most Pd catalysts reported in the literature, with lower activation enthalpies being compensated by more negative entropies of activation; as a result, the reaction is thermally compensated and the rate constants for most reactions are rather similar.

Experimental

Materials

The ImS3-14 surfactants were synthesized as described previously.[49] K$_2$PdCl$_4$ with a purity grade of 98% was purchased from Aldrich, Brazil. The chloroform used was distilled before use. Milli-Q water with a resistivity higher than 18.2 MΩ cm was used in all experiments. All other chemicals were of analytical grade and were used without any purification.
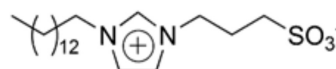
Figure 9. Chemical structure of ImS3-14 surfactant.

Preparation of palladium nanoparticles in reverse micelles

The palladium nanoparticles were synthesized at different water to surfactant concentration ratios (w$_0$), using the methodology previously described.[15,40] In fact, a water to surfactant concentration ratio of 4.8 was used for the preparation of Pd NPs 1. A higher ratio w$_0$ = 14.7 was needed for the preparation of Pd NPs 2.

The palladium nanoparticles obtained were characterized by transmission electronic microscopy (TEM). The samples for TEM analysis were prepared by deposition of the nanoparticle dispersion in a carbon-coated copper grid and analyzed in a JEOL JEM-2100 transmission electron microscope operating at 200 kV at LCME/UFSC, Florianópolis, Brazil.

Nanoparticles redissolution in water

The chloroform was removed through rotary evaporation and the black powder obtained was dissolved using a 0.08 mol L^{-1} NaCl aqueous solution. The solution was stirred until complete dissolution of the Pd NPs.

Palladium quantification

The quantification of palladium in the solutions was performed using energy dispersive X-ray fluorescence (EDXRF). The EDXRF measurements were performed using a S2 Ranger (Bruker, Germany) with temperature controlled to 23 ± 1 °C. Samples of 5 mL were placed in an X-Cell (with a diameter of 40 mm) and covered with a 5 μm thick polypropylene film, special for XRF analyses. The S2 Ranger measurements were carried out using a Pd X-ray tube, operated with Cu filter and 50 kV and 250 μm. An automatic sampler and EQUA ALL software were used for instrument control, data collection, and data analysis (Bruker, Gemany). Before analysis, instrument calibration and a stability check were performed.[40] For the nanoparticle synthesized in w_0 14.7 it was necessary to dilute the solution.

Kinetic studies of 4-nitrophenol reduction

The kinetic measurements were performed in a 3 mL quartz cell using a HP 8453 spectrophotometer operating in the range of 190-820 nm coupled to a thermostatic bath. First, were added an aliquot of 4-nitrophenol, an aliquot of palladium nanoparticle, 50 μL of 2.0 mol L^{-1} NaCl solution (to force the solubilization of nanoparticles) and an aliquot of water to complete 2 mL of solution. After cell thermostatting at 25 °C, the reactions were started by the addition of 1 mL of NaBH$_4$ solution, freshly prepared. Reactions were followed at 400 nm, referring to 4-nitrophenolate.

In this study, the 4-nitrophenol concentration was first varied from 0.006 to 0.12 mmol L^{-1}, keeping NaBH$_4$ and nanoparticle concentrations at 9.71 and 0.0167 mmol L^{-1}, respectively. Then the NaBH$_4$ concentration was varied from 0.83 to 15.8 mmol L^{-1}, keeping the 4-nitrophenol and nanoparticles concentrations at 0.093 and 0.0167 mmol L^{-1}, respectively. Finally, the nanoparticle concentration was varied from 0.0013 to 0.04 mmol L^{-1}, keeping the 4-nitrophenol and NaBH$_4$ concentrations at 0.093 and 9.71 mmol L^{-1}, respectively.

For the calculation of the thermodynamic activation parameters, rate constant (k_{app}) were determined at different temperatures. The concentration of reactants and catalyst were 0.093 mmol L^{-1} 4-nitrophenol, 9.71 mmol L^{-1} BH$_4^-$, 0.033 mmol L^{-1} NaCl and 0.0167 mmol L^{-1} Pd. The data were treated using the Eyring equation (equation 2):

$$k_{app} = \left(\frac{k_B T}{h}\right) \exp\left(\frac{}{R}\right) \exp\left(\frac{}{RT}\right) \qquad (2)$$

where k_{app} is the apparent rate constant (in s^{-1}), T is the temperature (in K), R is the universal gas constant (8.314472 J mol^{-1} K^{-1}), k_B is the Boltzmann constant (1.3806503 × 10^{-23} m^2 kg s^{-2} K^{-1}), h is Planck's constant (6.6261764 × 10^{-34} J s), $\Delta H^{\ddagger}$ is the enthalpy of activation and $\Delta S^{\ddagger}$ corresponds to the entropy of activation. From the values of $\Delta H^{\ddagger}$ and $\Delta S^{\ddagger}$, the Gibbs energy of activation ($\Delta G^{\ddagger}$) was calculated using equation 3:

$$\Delta G^{\ddagger} = \Delta H^{\ddagger} - T\Delta S^{\ddagger} \qquad (3)$$

Mass spectrometric study of the Nip reduction

The mass spectrometer system consisted of a hybrid triplequadrupole/linear ion trap mass spectrometer QTrap 3200 (Applied Biosystems/MDS Sciex, Concord, Canada) coupled to a Harvard Pump 11 Plus (Harvard Apparatus, Holliston, MA) for sample infusion. The experiments were performed using the Turbo VTM source (electrospray-ESI) in positive and negative ion mode. The capillary needle was maintained at 5500 V, and the declustering potential (DP) was set to 35 V. Synthetic air was used as nebulizer gas (GS1) at a pressure of 15 psi, and nitrogen was used at 10 psi as Curtain GasTM in the interface as well as collision gas (CAD GasTM) at 6 arbitrary units in the LINAC collision cell. The sample solution was diluted to 1.3 mg L^{-1} of Nip in water solution and infused at a rate of 10 μL min^{-1} using the built-in infusion pump. Then, electrospray mass and tandem mass experiments (MS2) were performed. The starting solution contained 0.093 mmol L^{-1} of 4-nitrophenol, 9.71 mmol L^{-1} NaBH$_4$, 0.033 mmol L^{-1} NaCl and 0.0019 mmol L^{-1} Pd and the aliquots were taken after the addition of NaBH$_4$.

General procedure for the reduction of aromatic nitro compounds with NaBH$_4$

A mixture of 3 mL of 0.015 mol L^{-1} aromatic nitro compound dissolved in tetrahydrofuran (THF), an aliquot of palladium nanoparticles, 300 μL of 2.0 mol L^{-1} NaCl solution and an aliquot of water were added into a reaction flask, totalizing 9 mL. Then, 900 μL of 0.5 mol L^{-1} NaBH$_4$ solution freshly prepared was added to the above solution under continuous stirring. The final ratio H$_2$O:THF was 2.3:1. The mixture was stirred at room temperature for 30 min. After this time, diethyl ether was added and the organic phase was separated and analyzed by gas chromatography (GC/MS) (chromatograph Agilent Technologies model 7820A coupled to mass spectrometer Agilent Technologies model 5975, operating with a column HP5-ms).

General procedure for the reduction of aromatic nitro compounds with H_2

In a Fischer-Porter glass flask, 0.9 mL of 0.015 mol L^{-1} aromatic nitro compound dissolved in THF, an aliquot of palladium and 90 µL of 2.0 mol L^{-1} NaCl solution was dispersed in 1.9 mL of H_2O. The reaction system was pressurized to 4 bars with hydrogen gas, followed by pressure release through an auxiliary bleed valve. This procedure was repeated three times to ensure the absence of other gases in the reaction vessel. The system was pressurized again at 4 bars, the mixture was vigorously stirred with a magnetic bar at 1500 rpm and the pressure was maintained constant. After 4 h, the pressure was released and diethyl ether was added to glass flask. The organic phase was separated and analyzed by GC/MS.

Supplementary Information

Supplementary data (TEM microscopy of Pd NPs, UV-Vis absorption spectra, ESI-MS and ESI-MS/MS spectrum and thermodynamics plots for reduction aromatic nitro compound) are available free of charge at http://jbcs.sbq.org.br as PDF file.

Acknowledgements

References

1. Jeong, C.; Park, J.; Bae, J. W.; Suh, Y. W.; *Catal. Commun.* **2014**, *54*, 1.

2. Kim, E.; Jeong, H. S.; Kim, B. M.; *Catal. Commun.* **2014**, *45*, 25.

3. Goesmann, H.; Feldmann, C.; *Angew. Chem., Int. Ed.* **2010**, *49*, 1362.

4. Pachon, L. D.; Rothenberg, G.; *Appl. Organomet. Chem.* **2008**, *22*, 288.

5. Kralik, M.; Biffis, A.; *J. Mol. Catal. A: Chem.* **2001**, *177*, 113.

6. Herves, P.; Perez-Lorenzo, M.; Liz-Marzan, L. M.; Dzubiella, J.; Lu, Y.; Ballauff, M.; *Chem. Soc. Rev.* **2012**, *41*, 5577.

7. Astruc, D.; Lu, F.; Aranzaes, J. R.; *Angew. Chem., Int. Ed.* **2005**, *44*, 7852.

8. Roucoux, A.; Schulz, J.; Patin, H.; *Chem. Rev.* **2002**, *102*, 3757.

9. Yan, N.; Xiao, C. X.; Kou, Y.; *Coord. Chem. Rev.* **2010**, *254*, 1179.

10. Nemanashi, M.; Meijboom, R.; *J. Colloid Interface Sci.* **2013**, *389*, 260.

11. Drinkel, E.; Souza, F. D.; Fiedler, H. D.; Nome, F.; *Curr. Opin. Colloid Interface Sci.* **2013**, *18*, 26.

12. An, K.; Somorjai, G. A.; *ChemCatChem* **2012**, *4*, 1512.

13. Reetz, M. T.; Helbig, W.; *J. Am. Chem. Soc.* **1994**, *116*, 7401.

14. Souza, B. S.; Leopoldino, E. C.; Tondo, D. W.; Dupont, J.; Nome, F.; *Langmuir* **2012**, *28*, 833.

15. Souza, F. D.; Souza, B. S.; Tondo, D. W.; Leopoldino, E. C.; Fiedler, H. D.; Nome, F.; *Langmuir* **2015**, *31*, 3587.

16. Fernandes, S. C.; de Souza, F. D.; de Souza, B. S.; Nome, F.; Vieira, I. C.; *Sens. Actuators, B* **2012**, *173*, 483.

17. Hwang, C. G.; Sang-Ho, K.; Hoon, O. J.; Kim, M. R.; Choi, S. H.; *J. Ind. Eng. Chem.* **2008**, *14*, 864.

18. Bhattacharjee, S.; Dotzauer, D. M.; Bruening, M. L.; *J. Am. Chem. Soc.* **2009**, *131*, 3601.

19. Campbell, P. S.; Santini, C. C.; Bayard, F.; Chauvin, Y.; Colliere, V.; Podgorsek, A.; Gomes, M. F. C.; Sa, J.; *J. Catal.* **2010**, *275*, 99.

20. Zhu, Y. J.; Zaera, F.; *Catal. Sci. Technol.* **2014**, *4*, 3390.

21. Miller, L.; Winter, G.; Baur, B.; Witulla, B.; Solbach, C.; Reske, S.; Linden, M.; *Nanoscale* **2014**, *6*, 4928.

22. Cuenya, B. R.; *Acc. Chem. Res.* **2013**, *46*, 1682.

23. Sadeghmoghaddam, E.; Gu, H. M.; Shon, Y. S.; *ACS Catal.* **2012**, *2*, 1838.

24. Zhong, R. Y.; Yan, X. H.; Gao, Z. K.; Zhang, R. J.; Xu, B. Q.; *Catal. Sci. Technol.* **2013**, *3*, 3013.

25. Li, Y.; El-Sayed, M. A.; *J. Phys. Chem. B* **2001**, *105*, 8938.

26. Ciganda, R.; Li, N.; Deraedt, C.; Gatard, S.; Zhao, P. X.; Salmon, L.; Hernandez, R.; Ruiz, J.; Astruc, D.; *Chem. Commun.* **2014**, *50*, 10126.

27. Dey, R.; Mukherjee, N.; Ahammed, S.; Ranu, B. C.; *Chem. Commun.* **2012**, *48*, 7982.

28. Gkizis, P. L.; Stratakis, M.; Lykakis, I. N.; *Catal. Commun.* **2013**, *36*, 48.

29. Corma, A.; Serna, P.; *Science* **2006**, *313*, 332.

30. Chen, L. F.; Hu, J. C.; Qi, Z. W.; Fang, Y. J.; Richards, R.; *Ind. Eng. Chem. Res.* **2011**, *50*, 13642.

31. Agrawal, A.; Tratnyek, P. G.; *Environ. Sci. Technol.* **1996**, *30*, 153.

32. Mirza-Aghayan, M.; Boukherroub, R.; Rahimifard, M.; Bolourtchian, M.; *Appl. Organomet. Chem.* **2010**, *24*, 477.

33. Corma, A.; Concepcion, P.; Serna, P.; *Angew. Chem., Int. Ed.* **2007**, *46*, 7266.

34. Pehlivan, L.; Metay, E.; Laval, S.; Dayoub, W.; Demonchaux, P.; Mignani, G.; Lemaire, M.; *Tetrahedron Lett.* **2010**, *51*, 1939.

35. Pogorelic, I.; Filipan-Litvic, M.; Merkas, S.; Ljubic, G.; Cepanec, I.; Litvic, M.; *J. Mol. Catal. A: Chem.* **2007**, *274*, 202.

36. Hudlicky, M.; *Reductions in Organic Chemistry*; 1st ed.; Ellis Horwood Limited: Chichester, 1984.

37. Wunder, S.; Polzer, F.; Lu, Y.; Mei, Y.; Ballauff, M.; *J. Phys. Chem. C* **2010**, *114*, 8814.

38. Wunder, S.; Lu, Y.; Albrecht, M.; Ballauff, M.; *ACS Catal.* **2011**, *1*, 908.

39. Zapp, E.; Souza, F. D.; Souza, B. S.; Nome, F.; Neves, A.; Vieira, I. C.; *Analyst* **2013**, *138*, 509.

40. Fiedler, H. D.; Drinkel, E. E.; Orzechovicz, B.; Leopoldino, E. C.; Souza, F. D.; Almerindo, G. I.; Perdona, C.; Nomet, F.; *Anal. Chem.* **2013**, *85*, 10142.

41. Signori, A. M.; Santos, K. D.; Eising, R.; Albuquerque, B. L.; Giacomelli, F. C.; Domingos, J. B.; *Langmuir* **2010**, *26*, 17772.

42. Saha, S.; Pal, A.; Kundu, S.; Basu, S.; Pal, T.; *Langmuir* **2010**, *26*, 2885.

43. Noh, J. H.; Meijboom, R.; *Appl. Surf. Sci.* **2014**, *320*, 400.

44. Bingwa, N.; Meijboom, R.; *J. Phys. Chem. C* **2014**, *118*, 19849.

45. Leger, B.; Nowicki, A.; Roucoux, A.; Rolland, J. P.; *J. Mol. Catal. A: Chem.* **2007**, *266*, 221.

46. Lu, Y. M.; Zhu, H. Z.; Li, W. G.; Hu, B.; Yu, S. H.; *J. Mater. Chem. A* **2013**, *1*, 3783.

47. Chen, J.; Zhang, Y.; Yang, L.; Zhang, X.; Liu, J.; Li, L.; Zhang, H.; *Tetrahedron* **2007**, *63*, 4266.

48. Viciu, M. S.; Grasa, G. A.; Nolan, S. P.; *Organometallics* **2001**, *20*, 3607.

49. Tondo, D. W.; Leopoldino, E. C.; Souza, B. S.; Micke, G. A.; Costa, A. C.; Fiedler, H. D.; Bunton, C. A.; Nome, F.; *Langmuir* **2010**, *26*, 15754.